Atmospheric Wake of Madeira: First Aerial Observations and Numerical Simulations

VANDA GRUBIŠIĆ*

National Center for Atmospheric Research,+ Boulder, Colorado

JOHANNES SACHSPERGER

Department of Meteorology and Geophysics, University of Vienna, Vienna, Austria

RUI M. A. CALDEIRA

Interdisciplinary Center of Marine and Environmental Research (CIIMAR), and Center for Mathematical Sciences (CCM), University of Madeira, Funchal, Madeira, Portugal

(Manuscript received 31 August 2014, in final form 10 August 2015)

ABSTRACT

The island of Madeira is well known for giving rise to atmospheric wakes. Strong and unsteady atmospheric wakes, resembling a von Kármán vortex street, are frequently observed in satellite images leeward of Madeira, especially during summer months, when conditions favoring the formation of atmospheric wakes occur frequently under the influence of the Azores high.

Reported here is the analysis of the first airborne measurements of Madeira's wake collected during the 2010 Island-induced Wake (I-WAKE) campaign. High-resolution in situ and remote sensing data were collected in the I-WAKE by a research aircraft. The measurements reveal distinctive wake signatures, including strong lateral wind shear zones and warm and dry eddies downwind of the island. A strong anticorrelation of the horizontal wind speed and sea surface temperature (SST) was found within the wake.

High-resolution numerical simulations with the Weather Research and Forecasting (WRF) Model were used to study the dynamics of the wake generation and its temporal evolution. The comparison of the model results and observations reveals a remarkable fidelity of the simulated wake features within the marine boundary layer (MBL). Strong potential vorticity (PV) anomalies were found in the simulated MBL wake, emanating from the flanks of the island. The response of the wake formation within the MBL to surface friction and enhanced thermal forcing is explored through the model sensitivity analyses.

1. Introduction

Atmospheric wakes leeward of isolated mountainous islands represent a zone of momentum deficit in stratified flow past isolated obstacles. The wakes are expected to be most distinctive in regions of sustained unidirectional winds in the presence of a strong marine boundary layer (MBL) inversion, lying at or below the mountain-top height. Such conditions prevail during summer months in the subtropical eastern Atlantic and provide key ingredients for the formation of atmospheric wakes generated by both the island of Madeira and the Canary Islands (Chopra and Hubert 1965; Zimmermann 1969). Madeira's wake was among the first to be identified in satellite imagery and documented in scientific literature (e.g., Hubert and Krueger 1962; Scorer 1986) owing to cloud formations within the subtropical stratus cover making the mesoscale flow structures within the wake easily identifiable (Fig. 1).

The first in situ observations within an atmospheric wake were collected during an airborne field campaign

Denotes Open Access content.

* Additional affiliation: Department of Meteorology and Geophysics, University of Vienna, Vienna, Austria.

+ The National Center for Atmospheric Research is sponsored by the National Science Foundation.

Corresponding author address: Vanda Grubišić, EOL, NCAR, P.O. Box 3000, Boulder, CO 80307.
E-mail: grubisic@ucar.edu

DOI: 10.1175/JAS-D-14-0251.1

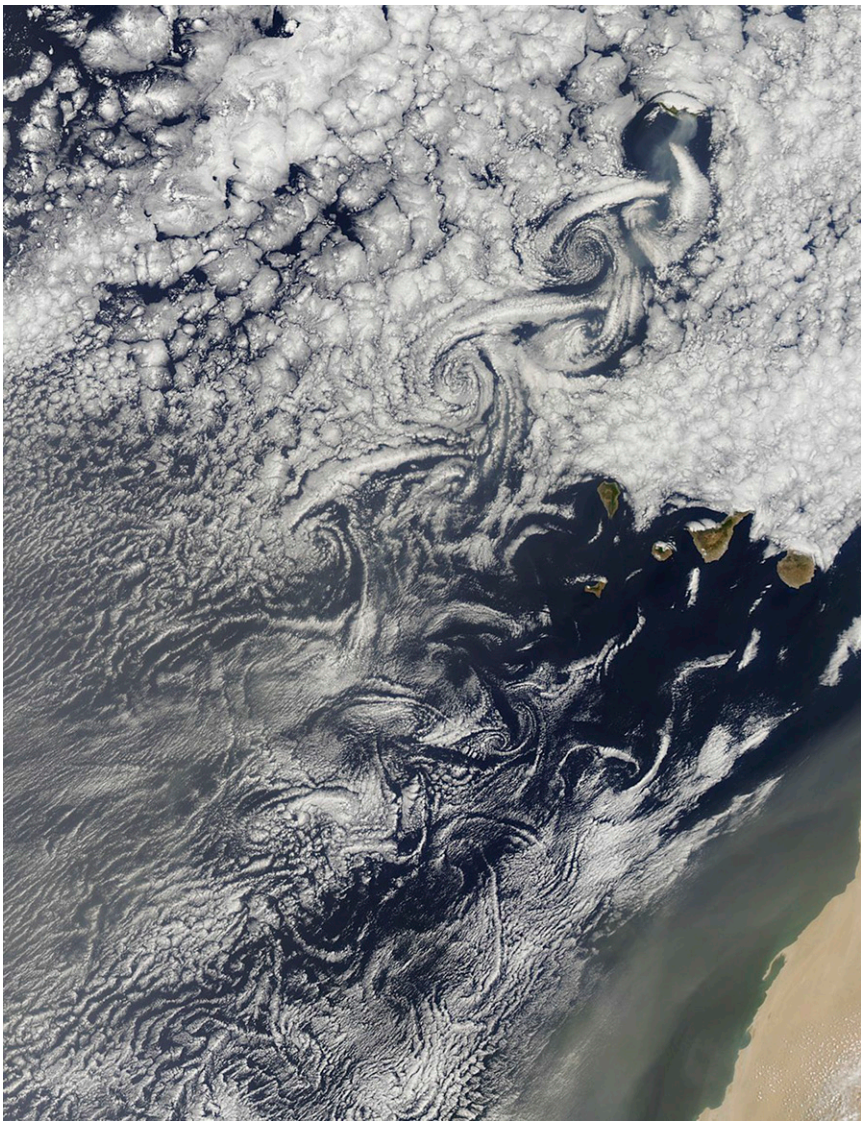

FIG. 1. NASA visible satellite image of a strong wake event on 21 Aug 2010. Unstable wakes from both the Madeira and the Canary Islands are made visible by the subtropical stratus formations, revealing the flow structure within individual wakes.

in Hawaii (Nickerson and Dias 1981). The analysis of the wind measured by aircraft in the near wake region of the island of Hawaii revealed a pair of counterrotating eddies there. A more in depth observational study of Hawaii's wake was carried out during the Hawaiian Rainband Project (HaRP) (Smith and Grubišić 1993). That study confirmed the earlier findings and showed Hawaii's wake to be quasi steady with two large counterrotating eddies extending some 150–200 km downwind from the island. In situ wake data were also collected leeward of the Caribbean island of St. Vincent (Smith et al. 1997). In all of these observational analyses, the wake appears as a zone of reduced momentum with sharp lateral shear lines—zones of strong horizontal wind shear—delineating the deceleration within the wake from the accelerated flow at the outer flanks. Positive potential temperature anomalies were found in the near wakes of all these islands. While the wake of the Big Island of Hawaii appeared to be quasi steady with two counterrotating eddies, the wake of St. Vincent was found to be rather weak and elongated without reversed flow or recirculating eddies leeward of the island. The evidence from satellite imagery and laboratory experiments (Etling 1989) shows that Madeira's wake is distinctly different from the above two in that its wake is unstable, displaying vortex shedding. Namely, in most of

the satellite images that appear in the literature, the flow past Madeira is shown to generate a vortex street that resembles a von Kármán vortex street from laboratory flows. The previous observational investigations of Madeira's wake have been primarily focused on its kinematics (Chopra and Hubert 1965; Zimmermann 1969; Young and Zawislak 2006). With the exception of a laboratory study by Etling (1989) and a recent numerical study by Caldeira and Tomé (2013), the dynamics of the Madeira wake generation has remained largely unexplored.

In this study we deliver the analysis of observational data that was collected in the wake of Madeira during the Island-induced Wake (I-WAKE) campaign, which took place in August–September 2010 as part of a larger ocean–atmosphere study that was focused on atmospheric and oceanic wakes generated by Madeira and air–sea interaction in the Madeira Archipelago. To the best of our knowledge, the data presented here represents the first in situ high-resolution aerial measurements obtained within the wake of Madeira. Furthermore, high-resolution numerical simulations with the Weather Research and Forecasting (WRF) Model are used to explore dynamical aspects of the wake generation and its temporal evolution.

In describing the generation and dynamical evolution of atmospheric wakes, one can resort to two dynamical frameworks: (i) the shallow-water model and (ii) the continuously stratified model. While not straightforward, the application of the shallow-water model to atmospheric flow past topographic obstacles has been done in describing a number of orographic phenomena including atmospheric wakes (Schär and Smith 1993a; Grubišić et al. 1995). The existence of a well-defined temperature inversion or an environmental critical level above and close to the mountain top promotes the decoupling of flow below and above such levels that, together with a well-mixed layer of near-neutral stability near the ground, makes the application of the shallow-water model to atmospheric island wake flows meaningful and relatively accurate (Jiang 2014).

In the shallow-water dynamical framework, with a strong temperature inversion near or below the mountain top, the shallow-layer flow largely splits around the obstacle. The momentum deficit in the wake and potential vorticity there result from the dissipation in hydraulic jumps, either in the immediate lee of the peak, in case of an inversion near the mountain top, or at the flanks of the obstacle for inversions below the mountain top. Once generated, the shear profile in the momentum deficit region of the wake is subject to convective and absolute instability that, for sufficiently strong momentum deficit, leads to vortex shedding (Schär and Smith 1993b). The generation of wakes in the continuously stratified flow past the obstacle has been extensively studied as well, through the application of theory, laboratory experiments, and idealized numerical simulations (Etling 1989; Smolarkiewicz and Rotunno 1989; Schär 1993; Schär and Durran 1997). The wakes are the hallmark of a nonlinear flow regime that is characterized by flow splitting upwind of an obstacle in a nearly horizontal flow and strong vertical vorticity and potential vorticity anomalies downwind of the obstacle. In this framework, the vertical vorticity of the wake originates through baroclinic generation and tilting in mountain waves and is further amplified through vertical stretching in the wave-breaking regions. Potential vorticity is formed by dissipative processes, either in the wave-breaking region aloft or in dissipation zones at or near the obstacle slopes (Rotunno et al. 1999; Epifanio and Durran 2002a,b). In this study, given the characteristics of the Madeira environment, we resort primarily to the shallow-water dynamical framework to describe different aspects of Madeira's wake generation and its dynamical evolution.

The paper is organized as follows. An overview of the geographic setting and climatological aspects of the flow past Madeira is presented in section 2. The I-WAKE campaign and the observational data used in this study are presented in section 3a. The numerical model and the experimental setup are described in section 3b. The observations and a detailed comparison with results of numerical simulations are presented in section 4. In section 5 we take a more in-depth look at some of the physical processes related to the wake dynamics. The study is summarized in section 6.

2. Terrain and climatology

a. *Terrain*

Madeira Islands is an archipelago of volcanic origin in the Atlantic Ocean that consists of two islands—Madeira Island and Porto Santo Island—and two groups of islands—the Desertas and the Selvagens (Fig. 2). The archipelago is located in the subtropical eastern Atlantic, approximately 850 km offshore from the southwest tip of Portugal to which the archipelago belongs politically. The island of Madeira, or Madeira for short, is the largest of the group. This northwest–southeast-oriented island is 55 km long and has a maximum width of 22 km. The island terrain rises steeply from the sea surface and takes shape of a northwest–southeast elongated mountain range. A large portion of that range reaches above 900 m MSL with the maximum height of 1862 m MSL at Pico Ruivo to the northwest of Funchal (Fig. 2). Compared to Madeira, Porto Santo (517 m, Pico do Facho) and the Desertas (442 m, Boqueiro Norte) are quite low

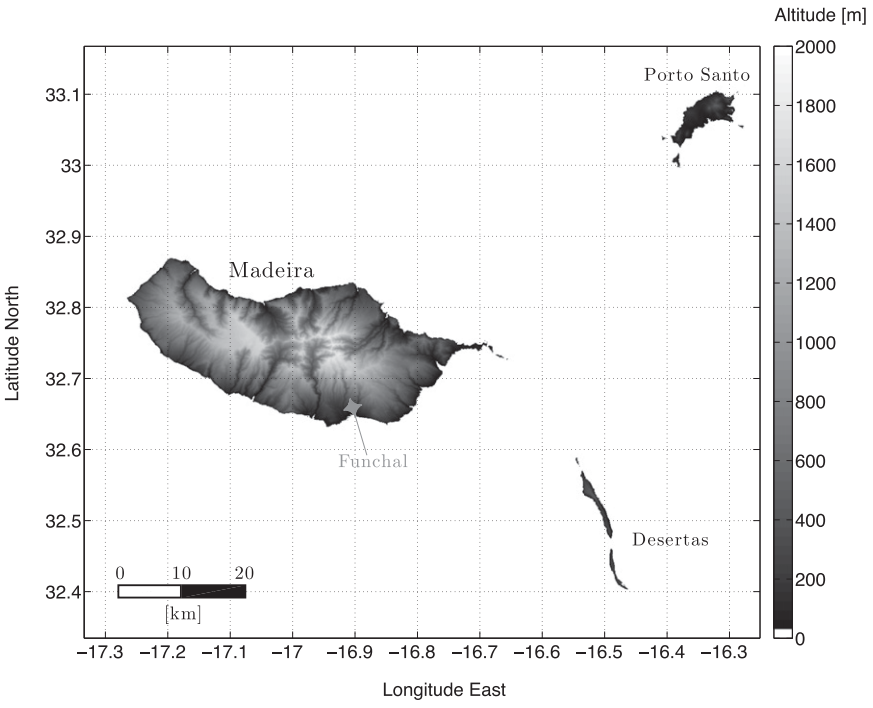

FIG. 2. High-resolution (90 m) terrain map of the Madeira Islands. The maximum height of Madeira, the largest island of the archipelago, is 1862 m MSL. The location of Funchal, the capital of Madeira and the operational sounding site, is marked with a gray diamond. The Selvagens are not shown in this map. During the I-WAKE campaign, the research aircraft operated out of Porto Santo. (Topography data source: NASA, Shuttle Radar Topography Mission (SRTM), version 2.1.)

and play only a minor role in the generation of airflow perturbations. The Selvagens are even lower than the Desertas and are too far downstream to have an appreciable effect on the flow past the archipelago.

b. *Climatology*

Because of its subtropical location at about 32.7°N, 17.0°W, Madeira is embedded in a larger-scale flow that is strongly influenced by the Azores high. The strength and location of this North Atlantic subtropical anticyclone has known annual variation (Davis et al. 1997).

The annual variation of the height and strength of the MBL inversion, derived from 1 yr (2010) of operational once-daily (1200 UTC) sounding data from Funchal, Madeira, is shown in Fig. 3. The most pronounced variation of the inversion heights in the Funchal sounding occurs from June to October, with much less variation displayed throughout the rest of the year. A gentle trend toward lower inversion heights starts in June, leading to the minimum in late August to early September. A steep rise from September to October brings the inversion heights back to the pre-June level.

Given Funchal's location at the lee coast of Madeira (32.63°N, 16.90°W, 58 m MSL, cf. Fig. 2), caution must be exercised in using this sounding as a proxy for undisturbed upstream environment. The comparison of the Funchal 1200 UTC soundings with the available upstream aircraft sounding and the ECWMF analyses shows a significant impact of terrain-induced perturbations on the Funchal wind profile, in particular below 1 km MSL, yet a relatively weak influence on the inversion height and strength. Quantitatively, the error in using the Funchal sounding as the proxy for the upstream environment falls below the error of the detection algorithm we have used to construct Fig. 3.

The 2010 data show that there are 117 days with temperature gradient exceeding 0.03 K m^{-1} and an inversion lying below 1500 m MSL, the latter being the height of the western Madeira plateau. That number is very close to 115 days yr^{-1} with an identifiable wake in the lee of Madeira that results from our climatological study of Madeira wake events, based on the analysis of visible satellite imagery in the time period 2003–10 (appendix). We note that the satellite climatology number is potentially an underestimate given that the presence of a wake was diagnosed exclusively from visible cloud patterns; that is, wakes under cloud-free days are not included in that number. Further details about the satellite climatology can be found in the appendix.

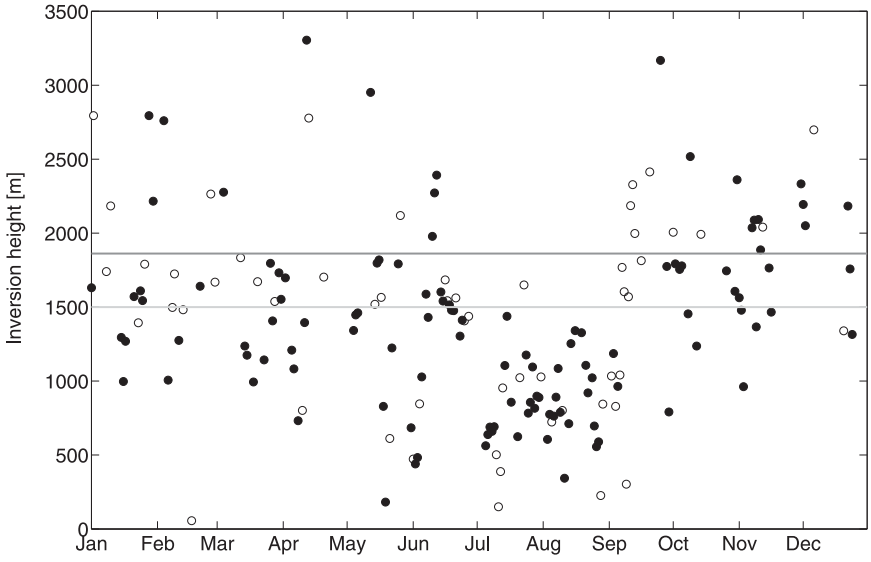

FIG. 3. Annual variation of the MBL inversion height derived from 1 yr (2010) of daily operational 1200 UTC Funchal soundings. Open circles indicate boundary layer inversions with a vertical potential temperature gradient of $0.03 < d\theta/dz < 0.06\,\mathrm{K\,m^{-1}}$. Solid circles denote inversions with $d\theta/dz > 0.06\,\mathrm{K\,m^{-1}}$. The two solid lines mark the height of the prominent terrain features on Madeira: Pico Ruivo, the highest peak at 1862 m MSL, and Paul da Serra, the western plateau at 1500 m MSL.

In summary, because of the position of the Azores high during summer months, the central mountain range of Madeira is oriented nearly perpendicular to the incoming northeast flow. This represents the most optimal orientation of that mountain range for generation of strong perturbations in airflow past Madeira. Furthermore, this is the time of year that strong trade wind inversions are mostly likely to lie below the height of the Madeira central mountain range. These two elements together constitute the optimal conditions for wake formation.

3. Observational data and numerical simulations

a. I-WAKE campaign

The data presented in this section were collected during the I-WAKE campaign, which took place in the Madeira Archipelago from 25 August to 5 September 2010. The measurement platforms deployed in I-WAKE include (i) a research vessel that measured oceanic vertical profiles and SST and (ii) the ATR-42 research aircraft, operated by Service des Avions Français Instrumentés pour la Recherche en Environnement (SAFIRE). The deployment of the ATR-42 to I-WAKE was supported by the European Facility for Airborne Research (EUFAR). The aircraft collected both the in situ and remote sensing measurements. The in situ data analyzed in this study has the temporal resolution of 1 Hz. The flight missions carried out during I-WAKE are listed in Table 1. The time difference between UTC and the local time in Madeira (western European summer time) during summer is +1 h.

In this study we analyze in detail a strong atmospheric wake event of 2 September 2010. The visible satellite image for this day, shown in Fig. 4, reveals relatively cloud-free conditions around Madeira. The first mission of the day was flown in the morning (IWAKE44) and consisted of one leg at 100 m MSL and one spiral sounding, both flown upstream of Madeira. The data from IWAKE44 was used to verify the I-WAKE operational mesoscale model (MM5) forecasts from the previous day before launching the afternoon wake survey mission (IWAKE45). The afternoon flight consisted of 10 straight legs flown within the wake region in the lawn-mower pattern at 100 m MSL plus a downstream spiral sounding. The emphasis in the wake survey was placed on low-level legs in order to obtain quality remotely sensed SST data. Together, these two research flights provide the highest spatial data coverage of a single wake event in I-WAKE. The IWAKE44 and IWAKE45 flight tracks and data sections used for model verification in this study are illustrated in Fig. 5.

Our analysis is based on the flight-level data for wind, temperature, and relative humidity and the remotely sensed SST from the quality-controlled dataset provided

TABLE 1. Research flight missions of the I-WAKE campaign. The time difference between UTC and the western European summer time is +1 h.

	Date						
	26 Aug	30 Aug	2 Sep		4 Sep		
Takeoff time (UTC)	1058	1342	0905	1334	0738	1233	1704
Duration (hh:mm)	04:12	04:24	01:00	04:30	00:54	00:53	00:54
Area of coverage	Whole wake	Three legs	One upstream leg	Whole wake	One downstream leg		
Soundings	1	2	1	1	0	0	0
Flight designation	IWAKE39	IWAKE42	IWAKE44	IWAKE45	IWAKE46	IWAKE47	IWAKE48

by SAFIRE. On the ATR-42 wind data are derived from the pressure measurements by the five-hole system (type Rosemount 1221) located at the radome of the aircraft, combined with the orientation of the aircraft (using the inertial navigation system) and the aircraft speed with respect to the ground (measured with the aircraft's global positioning system). Air temperature and humidity are measured, respectively, with a platinum resistance sensor (type Rosemount 102 E2AL) and a thermoelectric chilled mirror hygrometer (type General Eastern 1011B). SST data were derived from the downfacing radiometers [type Eppley Precision Infrared Radiometer (PIR)].

b. *Numerical model and experimental setup*

The WRF Model v3.3 with the Advanced Research version of WRF (ARW) dynamic core (Skamarock and Klemp 2008) was used for high-resolution numerical simulations in this study. ARW is a regional mesoscale model based on a set of fully compressible nonhydrostatic

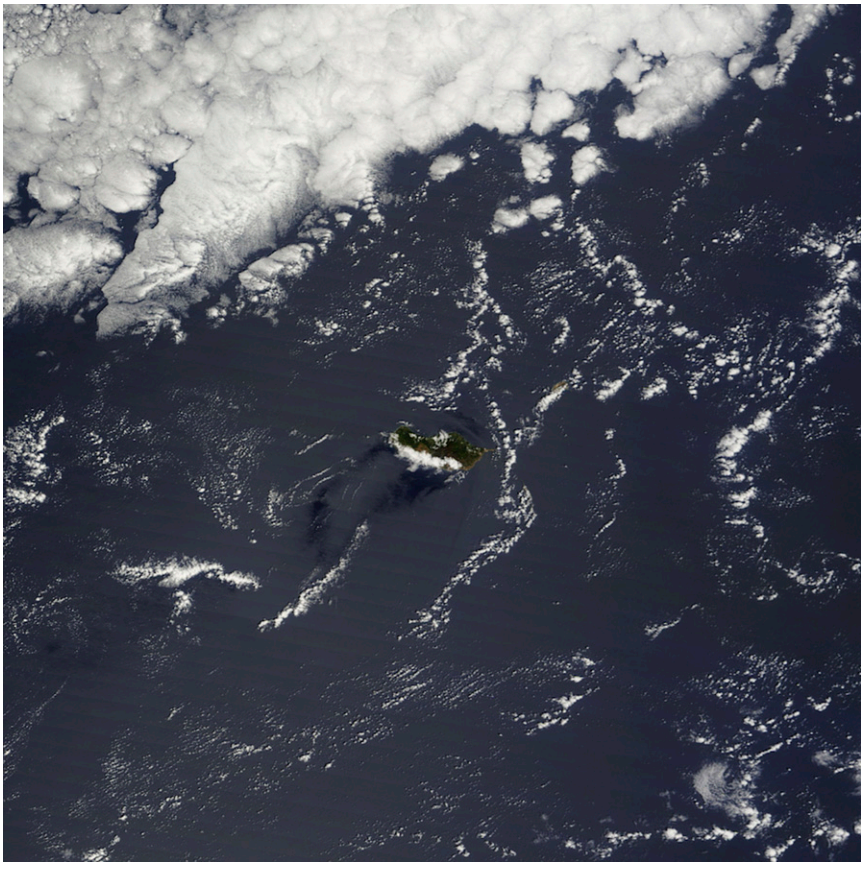

FIG. 4. The MODIS *Terra* visible satellite image zoom into the vicinity of Madeira at around 1400 UTC 2 Sep. Very few clouds are present and visible upwind and downwind of Madeira on this day. Dark signatures in the cloud-free parts of the image in the vicinity of Madeira represent areas of stronger specular reflection in the quietest parts of the wake.

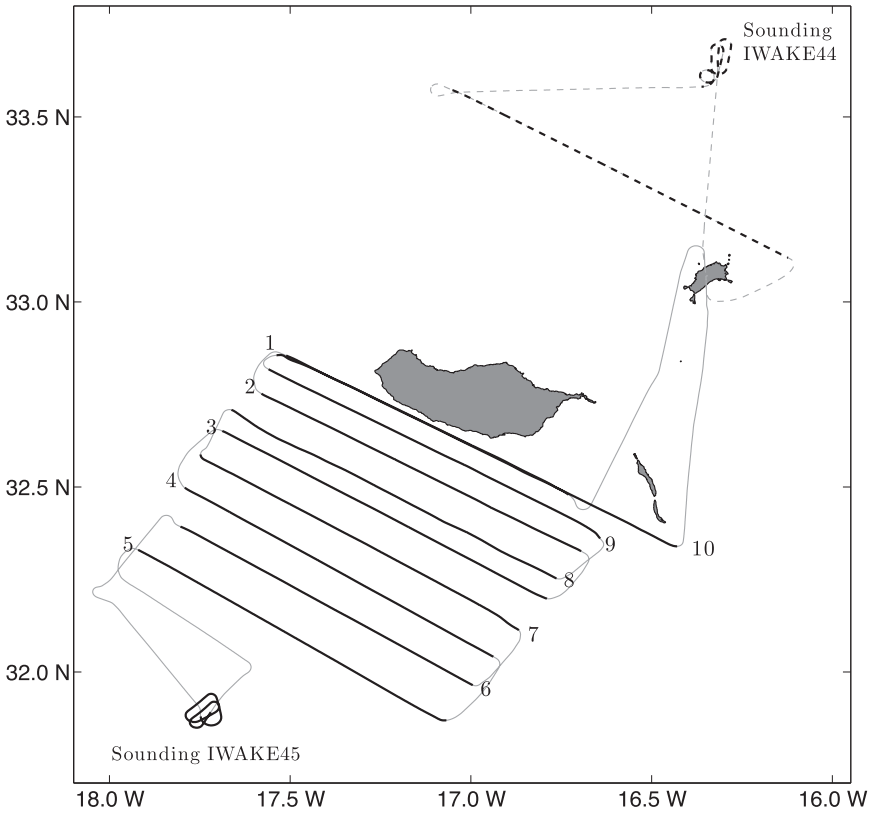

FIG. 5. Flight tracks of the research flights IWAKE44 (upstream morning survey, dashed gray) and IWAKE45 (afternoon wake survey, solid gray) flown on 2 Sep 2010. Subsections of these tracks employed in the analysis are shown in black. The 10 IWAKE45 flight legs are labeled sequentially, the increasing numbers reflecting the temporal sequence through which the legs were flown. The two flight legs nearest to Madeira (1 and 10) partly overlap. Gray shades indicate the land mask of the archipelago.

equations including moisture variables. The discretization consists of finite differences in space and a Runge–Kutta discretization scheme in time. A variety of physical parameterization schemes is available for representation of subgrid-scale physical processes. For real-case studies, initial and boundary conditions are intended to come from global or regional weather prediction models.

The model simulations of the 2 September wake event were carried out in a single domain, consisting of 500 × 500 grid points in the horizontal with a uniform horizontal grid spacing of 1 km. The island of Madeira was placed in the center of the domain. In the vertical, 59 unequally spaced sigma levels were placed between the ground and the model top at 20 km. Except in the vicinity of the inversion, the vertical spacing of sigma levels increases nearly linearly in the lowest 3 km of the domain, from 85 m at the first model level (at 42 m) to approximately 110 m at the height of 3 km. To better resolve the inversion (≈1000 m MSL), the density of sigma levels was increased in its proximity, resulting in the minimum vertical grid increment there of approximately 45 m. Above 3 km, the sigma-level spacing was set to increase exponentially with height, reaching approximately 1 km at the tropopause.

All simulations were initialized at 0600 UTC 1 September 2010 and carried out for 42 h. Initial and boundary conditions for the WRF simulations were obtained by interpolating to the model grid the operational ECMWF analyses data, available at 6-hourly intervals at the horizontal resolution of 0.25° and 91 vertical atmospheric levels. Using the original ECMWF fields, the WRF simulation predicted colder-than-observed conditions within the marine boundary layer and the wake region. To correct for this discrepancy, in the control run (WE1 in Table 3) the SST from the ECMWF analysis was increased uniformly by 1 K.

The selected physical parameterization schemes for the numerical experiments in this study are listed in

TABLE 2. Selected subgrid-scale parameterizations for the WRF runs.

Physics	Scheme
Microphysics scheme	WRF single-moment 6-class microphysics scheme (WSM6; Hong and Lim 2006)
Longwave radiation scheme	Rapid Radiative Transfer Model (Mlawer et al. 1997)
Shortwave radiation scheme	Rapid Radiative Transfer Model for GCM (Iacono et al. 2008)
Interval of radiative physics	30 min
Surface-layer physics	Eta similarity (Janjić 1994)
Land surface physics	Noah land surface model (Niu et al. 2011)
PBL physics	Mellor–Yamada–Janjić (Janjić 1994)
Cumulus parameterization	Turned off
Urban physics	Turned off
Nonhydrostatic	True

Table 2. Two sets of sensitivity experiments were performed in order to explore the impact of (i) thermal forcing at the lower boundary on the upstream stratification and, in turn, on the simulated flow and (ii) surface friction on the wake formation. The skin temperature, which is used for the computation of surface-layer momentum and heat fluxes in the Mellor–Yamada–Janjić (MYJ) scheme, was selected as the control parameter for thermal forcing at the sea surface. In the related sensitivity experiments, this parameter was modified over the range $[-2.5, 2.5]$ K over water only, the adjustment being done in the preprocessing stage of the numerical runs. The advection time from the lateral boundaries to the center of the domain was found to be sufficiently long for the convective MBL to adjust fully to the modified lower-boundary thermal forcing before reaching the island. In the surface friction sensitivity experiment, the momentum exchange coefficient at the surface was set to zero within the surface-layer parameterization. This has an effect of switching off surface drag in the momentum exchange while leaving the heat exchange part of the parameterization unaffected. All numerical experiments reported in this study are listed in Table 3.

4. Observational data analysis and comparison to control simulation

a. *Analysis of observations*

1) SOUNDINGS

The operational Funchal soundings during the period 1–3 September 2010 show a continuous strengthening of the MBL inversion and the attendant change of the vertical stability structure, from a nearly uniformly stratified atmosphere at the beginning of this period to a layered structure, more characteristic of the subtropical marine atmosphere, toward the end of this period.

The vertical profiles of wind speed, wind direction, and potential temperature sampled during the IWAKE44 (upwind) and IWAKE45 (downwind) spiral soundings on 2 September 2010 are shown in Fig. 6. We do not show the humidity profiles as, given very few clouds that were observed on this day, we expect moisture and clouds to play a very minor role in this problem. The upstream sounding (Fig. 6a) was initiated at 0915 UTC and carried out upwind of Porto Santo to collect data needed to characterize the incoming flow. The downwind sounding (Fig. 6b), initiated at 1545 UTC, approximately 120 km downstream of Madeira, represents a sample of the vertical structure of the atmosphere in the disturbed part of the flow within the wake.

The upwind aircraft sounding of 2 September 2010 presents a typical layered subtropical marine atmospheric structure with a sharp and thin temperature inversion ($\Delta\theta = 7$ K) at 1000 m MSL. The vertical gradient of potential temperature across the inversion is $\partial\theta/\partial z = 0.03\,\mathrm{K\,m^{-1}}$. The inversion separates two distinct atmospheric layers: (i) a well-mixed MBL with uniform potential temperature ($\theta = 295$ K) underneath the inversion and (ii) a stratified layer above the inversion with $\partial\theta/\partial z \approx 8.5 \times 10^{-3}\,\mathrm{K\,m^{-1}}$. The well-mixed nature of MBL is reflected also in the horizontal wind speed profile with $U_\infty = 5\,\mathrm{m\,s^{-1}}$ within this layer. The wind direction within the MBL is less uniform, turning from northeast (≈45°) near the sea surface to north (0°) at 800 m MSL and back to northeast below the inversion. Both the wind speed and direction are rather uniform in

TABLE 3. List of performed WRF simulations. SST offset is with respect to the SST value in the operational ECWMF analysis.

Label	Description
WE-2.5	Uniform SST offset by −2.5 K
WE0	Uniform SST offset by 0 K
WE1	Uniform SST offset by +1 K (Control run)
WE2.5	Uniform SST offset by +2.5 K
FS	As in WE1, but with free-slip conditions

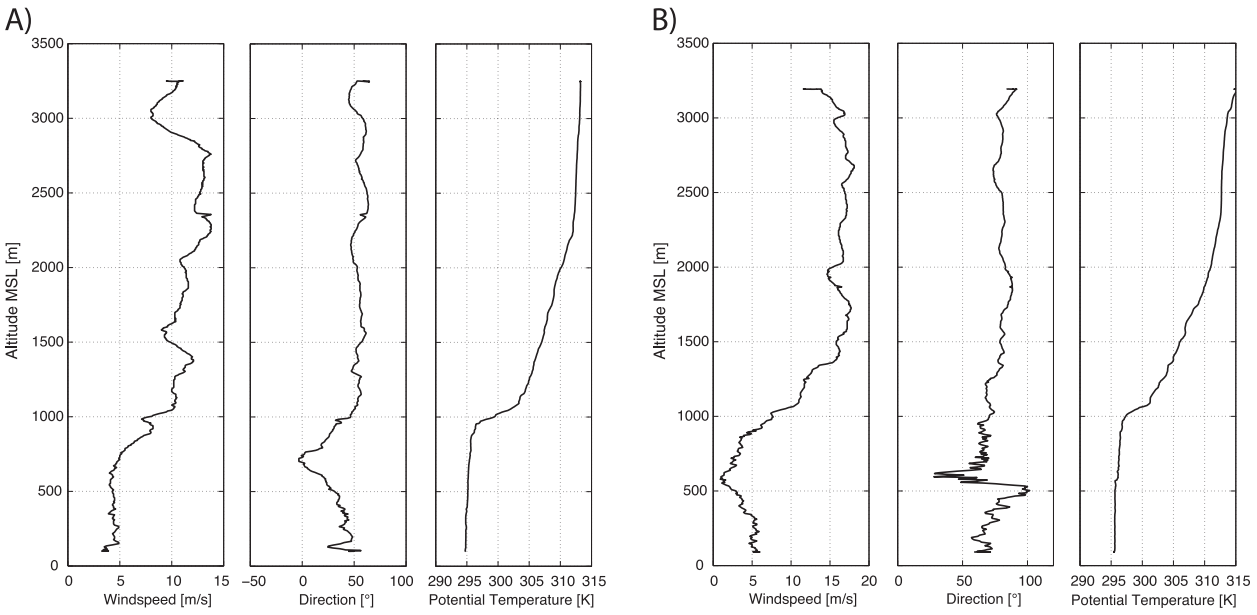

FIG. 6. Wind speed (m s^{-1}), wind direction (°), and potential temperature (K) profiles from the two spiral soundings on 2 Sep 2010 carried out during (a) IWAKE44 (sounding initiated at 0915 UTC) and (b) IWAKE45 (sounding initiated at 1545 UTC). The corresponding sounding locations are marked in Fig. 5. The length of each spiral sounding was approximately 10 min.

the stratified layer above, with the northeast (≈50°) wind at approximately $U_\infty = 10\,\mathrm{m\,s^{-1}}$.

The downstream sounding displays these general characteristics as well but it also reflects modifications due to flow past the island. The temperature jump across the MBL inversion at 1000 m is weaker. The MBL downwind of the island is slightly warmer (by <1 K) than upstream. Also, it is divided into two sublayers by a micro inversion of approximately 0.5 K at 560 m MSL. This layering is evident also in the wind speed and wind direction. Whereas the wind speed below the micro inversion is the same 5 m s^{-1} as in the upstream MBL, the flow in the layer between the two inversions is significantly slower, with wind speed being nearly zero there. The wind in the stratified layer above the main inversion—east-northeast (75°) exceeding 15 m s^{-1}—is also noticeably different downstream of the island.

Using the wind speed and potential temperature within the MBL, together with the height of the MBL inversion and the temperature jump across it, one can estimate the ambient Froude number

$$\mathrm{Fr} = \frac{U_\infty}{\sqrt{g'H}} = 0.33, \qquad (1)$$

where $g' = g\Delta\theta/\theta = 0.232\,\mathrm{m\,s^{-1}}$ is reduced gravity and H represents the depth of a shallow fluid layer below the MBL inversion. Using the height of the Madeira western plateau ($h_m = 1500$ m) for obstacle height, the ratio of the mountain height to layer depth is $M = h_m/H = 1.5$. The values of these two parameters for the 2 September 2010 event place the flow past Madeira well into the strong wake regime of two-dimensional shallow-water flow past an isolated obstacle (Fig. 7), within which a reversed flow and wake vortices are expected to form.

2) HORIZONTAL WAKE STRUCTURE

The horizontal wind, potential temperature, and SST measured along the IWAKE45 flight legs at 100 m MSL are shown in Figs. 8 and 9. For the ease of interpretation, we have separated the data collected along the outbound and returns legs of this 4.5-h-long wake flight. Both the potential temperature and the SST anomalies in these figures represent the difference between the local value of these fields and the measured minimum along each of the wake flight legs. That is, $\theta_a(t_{\mathrm{obs}}) = \theta(t_{\mathrm{obs}}) - \theta_{\mathrm{min}}$ and $\mathrm{SST}_a(t_{\mathrm{obs}}) = \mathrm{SST}(t_{\mathrm{obs}}) - \mathrm{SST}_{\mathrm{min}}$.

The wake can be identified as a generally calmer region in the lee of the island, with stretches of reversed flow near the center of the first few flights legs closest to the island. It is along those legs that one can most clearly see the lateral shear lines separating the wake from the accelerated flow to the side of it. Our observations capture more of the accelerated flow on the south side of the island, showing its far downwind extent. The wind measurements in Figs. 8a and 9a are consistent with the satellite image in Fig. 4 and the visual observations of

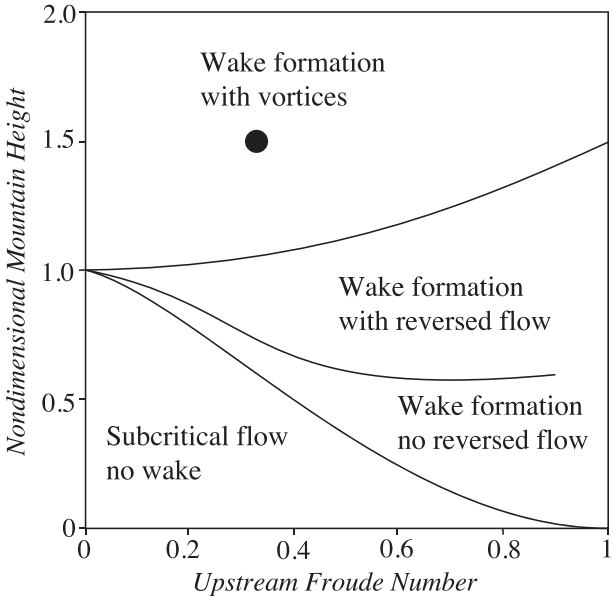

FIG. 7. Regime diagram for shallow-water flow past an isolated obstacle [after Schär and Smith (1993a)]. The black dot indicates conditions for Madeira that were estimated using the IWAKE44 sounding data and the height of the Madeira western plateau.

the state of the ocean surface from the IWAKE45 research flight (not shown). The strong gradients of the horizontal wind speed at the lateral shear lines are reflected in the distinctly different state of the ocean surface on the two sides of these lines—the mirror-like undisturbed sea surface inside the most sheltered parts of the wake and the white-cap-covered sea surface underneath the accelerated airflow outside the wake. In the satellite image, the former appear as dark sea surface patches that stand in contrast to other cloud-free parts of the wake. An orographic cloud seems to form on the leeside of the island, where the wake-reversed flow meets the island terrain and pushes the wake air up the steep leeside slopes. Last, a linear cloud feature farther in the wake appears to form along the wake shear line at the south side of the wake. The wind observations in Figs. 8a and 9a provide little to no indication that this wake is either symmetric or steady.

The largest potential temperature anomalies along these flight legs lie within the sheltered parts of the wake (Figs. 8b and 9b). The peaks, exceeding in places +1 K, are found on the wake side of the lateral shear lines. This is most clearly evident along the adjacent legs 3 and 8, where the maxima of the temperature anomaly coincide with the sharp turns in the wind direction, suggestive of the center position of a wake eddy (cf. Figs. 8a and 9a). The anomaly along the outbound leg 3 is stronger near the leg midpoint, at the center of what appears to be an anticyclonic eddy, whereas one along the return leg 8 is stronger at the NW end of that leg, at the center of what appears to be a cyclonic eddy. It should be noted that the time difference between these two legs is 2 h 15 min. Furthermore, these positive temperature anomalies within the wake are collocated with negative anomalies of relative humidity (not shown), suggesting an inclusion of potentially warmer and drier air above the inversion at the center of the eddies.

The impact of Madeira's terrain is not limited only to the atmospheric flow leeward of the island but extends also to the ocean surface. In Figs. 8c and 9c, shown is the remotely sensed SST during the IWAKE45 flight. A strong anticorrelation of SST and wind speed is clearly evident, with higher values of SST in regions of reduced horizontal wind speed and vice versa. This anticorrelation is most pronounced along the return flight leg 10 closest to the island. This is despite the fact that the downwelling shortwave radiation there diminished by clouds in the MBL during the course of the flight, from 800 W m^{-2} on the outbound leg 2 (≈1400 UTC) to approximately 400 W m^{-2} on the return leg 10 (≈1730 UTC).

b. Comparison to control simulation

To conduct a meaningful comparison between the observations and the simulation results in what appears to be an unsteady flow, the flight track within the wake was divided into 10 straight segments, each approximately 15 min in length (cf. Fig. 5). Furthermore, the model output was saved every 15 min. For each of the horizontal flight segments, the time of the model output corresponds closely to the center of each flight leg. For vertical profiles, that time falls at the start of the aircraft spiral sounding. In this analysis, we assume that the flow is approximately steady on the time scale of 15 min, allowing us to compare a snapshot of the model output with a continuous time series of observations. Trilinear interpolation of the control run output was used to obtain model-predicted values at discrete points along the flight tracks. The model soundings were extracted along a straight vertical line in the center point of the spiral aircraft soundings (cf. Fig. 5).

In Fig. 10, shown is the comparison between the IWAKE44 upstream sounding profile with the soundings from the WRF control simulation and from the ECMWF model, the latter linearly interpolated in time to the time of the aircraft sounding. Both the WRF and the ECWMF profiles provide a good representation of the observed profiles in the free troposphere above the MBL inversion, with the WRF providing a somewhat more accurate wind speed profile than the ECWMF

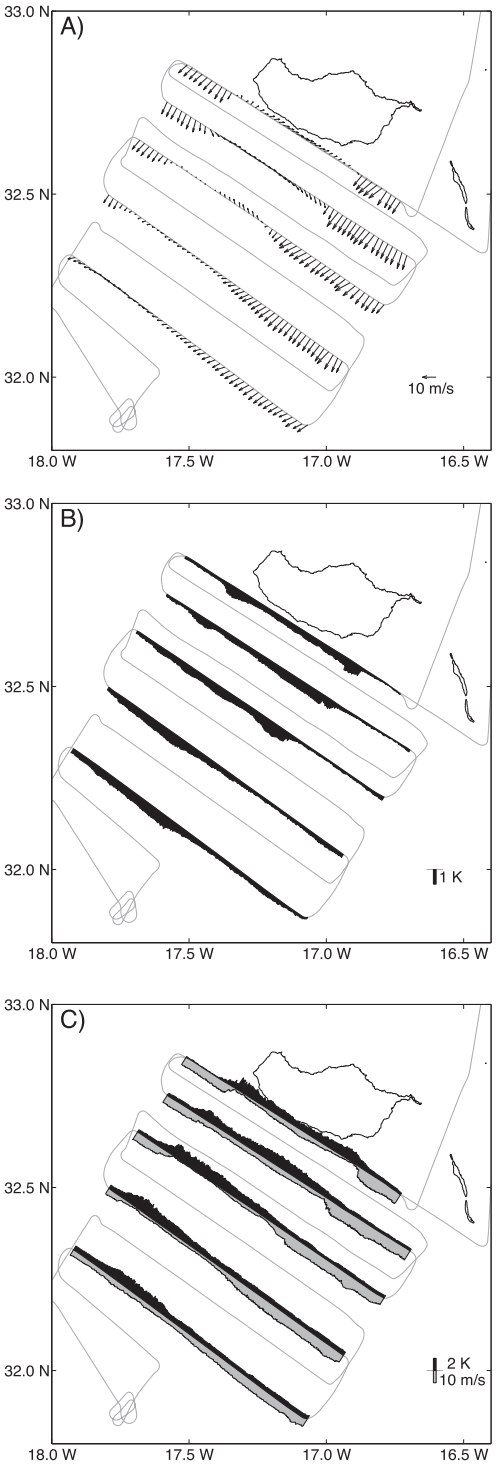

FIG. 8. (a) Horizontal wind vectors (legend arrow = 10 m s^{-1}), (b) potential temperature anomaly (legend symbol = 1 K), and (c) wind speed (gray, legend symbol = 10 m s^{-1}) and SST anomaly (black, legend symbol = 2 K) for the outbound legs (1–5) of the IWAKE45 flight. Anomalies represent the difference between local values and the measured minimum along each of the wake flight legs. Black irregular lines mark the islands' coastlines. The flight tracks are shown with gray solid lines. All wake legs were flown at 100 m MSL.

model. Within the MBL, the differences between both the WRF and the ECMWF predictions and the observations are more pronounced, with both models overpredicting the trade wind speed by nearly 2 m s^{-1} and underpredicting the MBL temperature by close to 1 K. The WRF temperature profile offers an improvement over the ECMWF profile in the inversion zone, with a better formed and sharper inversion. The temperature jump across that inversion is 2 K stronger and its base 100 m higher than the observed, resulting in a sharper delineation of the MBL and the free troposphere.

In Figs. 11–13, the observed and the WRF-simulated along- and cross-stream horizontal wind components and potential temperature are shown along the 10 flight legs, revealing a close agreement between the observed and the simulated wake features. The agreement is particularly close along the flight legs closest to the island (legs 1 and 10), where the wake structure is reproduced very accurately, including both the spatial structure and magnitude of the horizontal shear of the two horizontal velocity components. The same applies to the thermal structure of the wake that shows only slightly more discrepancy between the model predictions and the observations (Fig. 13). Further examination of the model results shows that the wake is contained fully underneath the MBL inversion.

5. Process studies

Having established that the WRF control run closely reproduces the observed upstream atmospheric structure and the wake features allows us to use the model simulations for further analysis of physical processes involved in the generation and dynamic evolution of Madeira's wake. In this section, we explore the impact of thermal forcing at the sea surface on the upstream stratification and, in turn, on the simulated flow—as well as surface friction on the wake formation. Furthermore, we examine the period of vortex shedding in Madeira's wake.

a. Impact of sea surface temperature

In the study of a 2002 strong Madeira wake event, Caldeira and Tomé (2013) showed that the increase in SST has a significant impact on the simulated wake flow regime via the erosion of the lower atmospheric stratification. In this study, we examine the effect of thermal forcing at the sea surface on the simulated structure of the MBL and the trade wind inversion by varying the difference between the applied SST and the ECMWF SST field over the range [−2.5, 2.5] K (cf. section 3b and

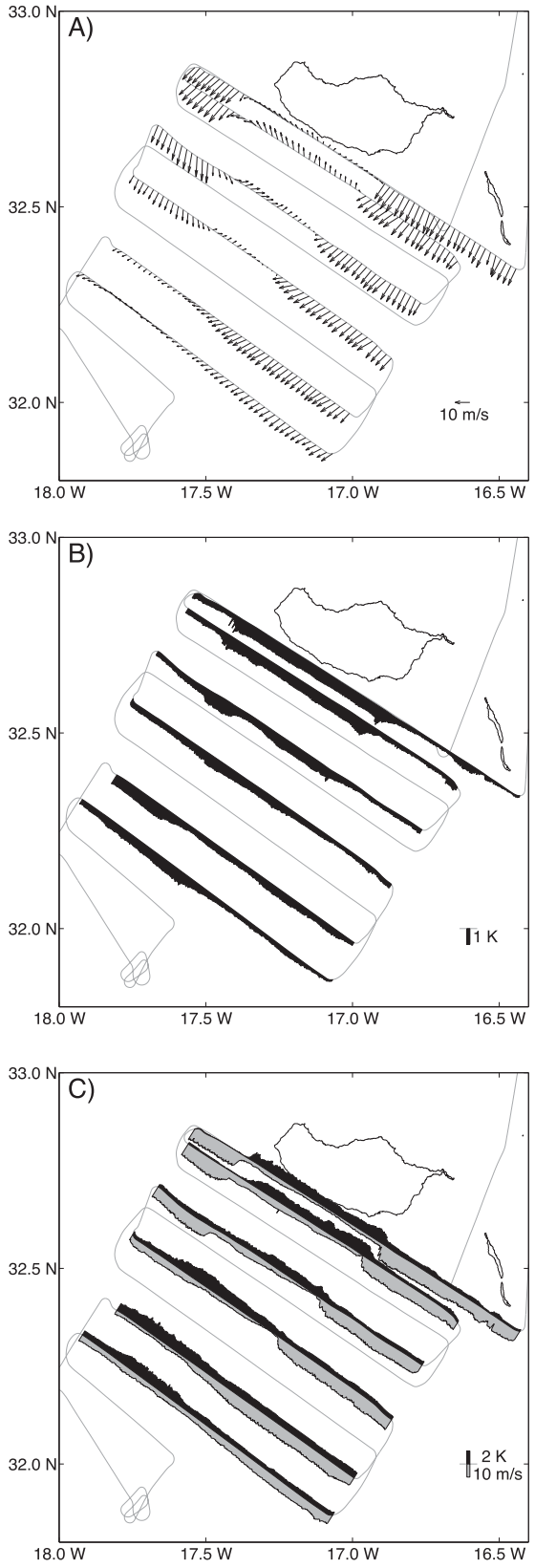

FIG. 9. As in Fig. 8, but for the return legs (6–10) of the IWAKE45 flight.

Table 3 for details). As a quantitative measure of the effect of SST on the fidelity of the WRF simulation, we calculated the root-mean-square error [RMSE; Eq. (2)] of the horizontal wind components and potential temperature along the 10 wake flight legs. The RMSE was computed using

$$\mathrm{RMSE} = \sqrt{\frac{1}{N}\sum_{i=1}^{N}[\psi_{\mathrm{obs}}(i) - \psi_{\mathrm{sim}}(i)]^2}, \qquad (2)$$

where N is the number of data points along a flight leg and ψ_{obs} and ψ_{sim} are the observed and simulated values of a physical quantity. The RMSE was calculated for all three of the physical parameters selected (u, v, θ) and for each flight leg. The RMSE values for the four experiments in this series are shown in Fig. 14a. It is evident that the control run (WE1) has the best score, featuring the lowest mean RMSE value and the smallest spread of the RMSE values for all three of the selected parameters. Of the three physical quantities examined, this is most clearly evident in the RMSE for potential temperature.

From the upstream vertical profiles of potential temperature obtained for different values of SST (Fig. 14b), it is evident that the increase in SST leads to the higher and sharper inversions. This result is consistent with higher SSTs leading to stronger surface heat fluxes for a given fixed MBL temperature, forcing more vigorous vertical mixing and resulting in a thicker marine boundary layer and a sharper inversion at its top. We also note that in all the runs except WE-2.5, SST is higher than the potential temperature within the steady-state MBL (cf. Fig. 14b). This suggests that the impact of the increased surfacing heating is of secondary importance in the overall heat budget within the MBM. Indeed, an evaluation of the energy balance over water surfaces shows that the largest portion of the available energy in the surface energy budget is taken up by evaporation of surface water rather than by direct heating of the boundary layer. Consequently, the latent heat flux is an order of magnitude larger ($\approx 100\,\mathrm{W\,m^{-2}}$) than the sensible heat flux ($\approx 10\,\mathrm{W\,m^{-2}}$) and it is possible to maintain a steady state in the MBL despite the SST that is nearly 3 K warmer than the overlying air within the MBL. However, even that small amount of sensible heat flux increases slightly the potential temperature in the MBL and, in runs with higher SSTs, leads to a reduced discrepancy in the potential temperature between the model and the observations.

The relatively modest changes to the upstream stability structure over the examined range of SSTs clearly

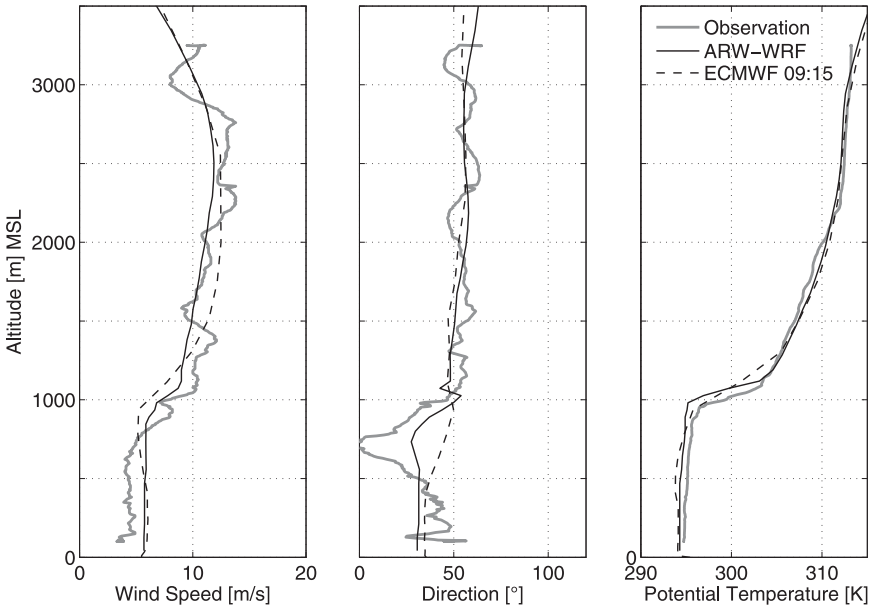

FIG. 10. Comparison of (left to right) wind speed, wind direction, and potential temperature profiles from the ECMWF model (dashed) and the WRF control run (solid black) at 0915 UTC 2 Sep 2010 with the measured profiles (solid gray) in the research flight IWAKE44 during the spiral sounding upstream of Madeira.

have an effect on the fidelity of simulations as is evident from the mean and spread of the RMSE values for the 10 wake legs in Fig. 14. While both horizontal wind components show a larger spread of RMSE values than is the case for potential temperature, it is the cross-stream component in particular that appears to be sensitive to the SST. That wind component carries most of the information on details of the wake circulation, including the position of the wake eddies and the phase of the eddy shedding. Thus, it would appear that while the overall flow morphology is not significantly affected by the SST over the examined range, the circulation within the wake interior, including the phase of the eddy shedding, is.

b. *Impact of surface friction*

The examination of the simulated flow field for 2 September 2010 at 600 m MSL, during the time of the IWAKE45 research flight (Fig. 15), reveals a flow splitting upwind of Madeira and an asymmetric flow structure leeward of the island, with multiple cyclonic and anticyclonic vortices within the wake. The time of the two panels in Fig. 15 corresponds approximately to the beginning of the outbound portion and the end of the return portion of the wake flight. The vertical vorticity field (ζ) shown in these panels clearly indicates that there is a concentration of vertical vorticity within the vortex centers and along the lateral shear lines, in particular at the flanks of the obstacle in the near wake. The strong concentration of vertical vorticity at the lateral shear lines is consistent with the sharpness of the horizontal shear along legs 1 and 10 (top rows in Figs. 11 and 12). The anticyclonic and cyclonic eddies whose existence one can infer from observations in Figs. 8 and 9 are clearly visible in Fig. 15.

As a kinematic quantity, vertical vorticity is perfectly suited for the analysis of the kinematic structure of the wake. For locating the sources of vorticity within the Eulerian framework of the numerical model, whose equations contain the basic physics that describe the generation of vorticity one finds in the simulated wake, vertical vorticity is more difficult to use, owing to its nonconservative nature, than its conservative counterpart—the potential vorticity (Rotunno et al. 1999). For a three-dimensional (3D) flow field, potential vorticity is defined as

$$\mathrm{PV} = \frac{1}{\rho}\boldsymbol{\omega} \cdot \nabla\theta, \tag{3}$$

where $\boldsymbol{\omega} = (\xi, \eta, \zeta)$ is the 3D vorticity vector and θ and ρ are, respectively, potential temperature and air density. In the absence of diabatic and dissipative processes, potential vorticity is a conserved quantity (Gill 1982). Consequently, potential vorticity in a flow downwind of an obstacle in which there is no PV upstream implies

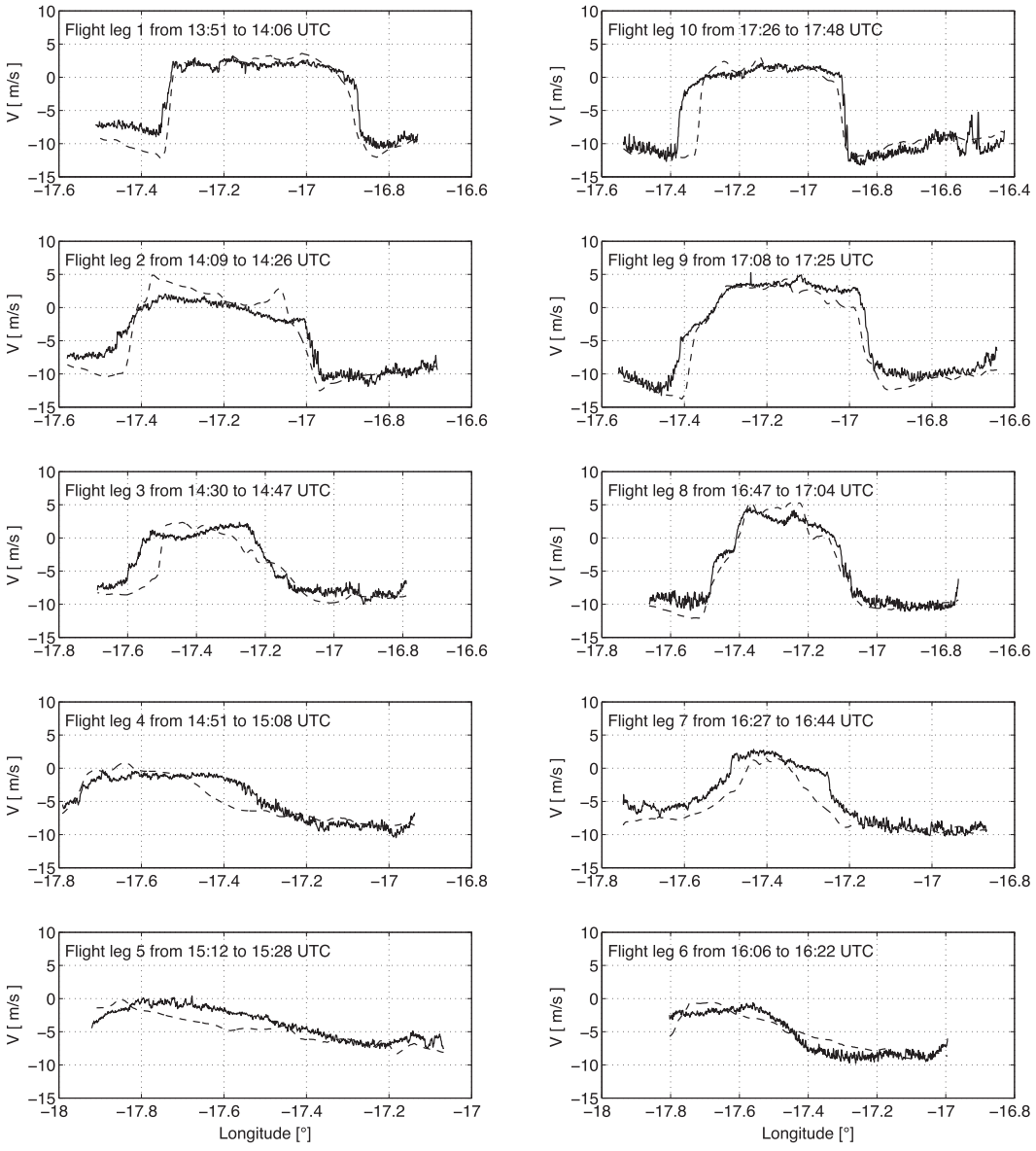

FIG. 11. Comparison of the observed (solid) and the WRF-simulated (dashed) along-stream wind component for the 10 wake flight segments of the flight IWAKE45 at 100 m MSL (cf. Fig. 5). (top to bottom) The distance from the island increases, with the top two panels displaying the flight legs (1 and 10) closest to Madeira.

that either diabatic or dissipative processes have been encountered along the way as the air passed the obstacle. In the left column of Fig. 16, shown are the streamlines and potential vorticity at 600 m MSL as well as the potential temperature perturbation at 50 m MSL from the control run at 1200 UTC 1 September 2010, 6 h after the initialization of the control simulation. It is apparent from these panels that the flow splitting is present at low levels. It is also apparent that there is no potential vorticity within the MBL upwind of Madeira, as one would expect to be the case based on Eq. (3) for a well-mixed subtropical MBL ($\nabla\theta \approx 0$). Downwind of Madeira, the extrema of potential vorticity (PV), with values between -10 and $+10$ PV units (1 PVU = 10^{-6} K kg^{-1} m^2 2 s), are clearly evident.

The friction enters the vertical vorticity budget through horizontal gradients of the friction force. As shown in Grubišić et al. (1995), it is reasonable to expect that the horizontal gradient of friction over the island terrain and, in particular, along the steep coastline, at the transition between land and sea surface, have a significant impact on the wake formation. To test this

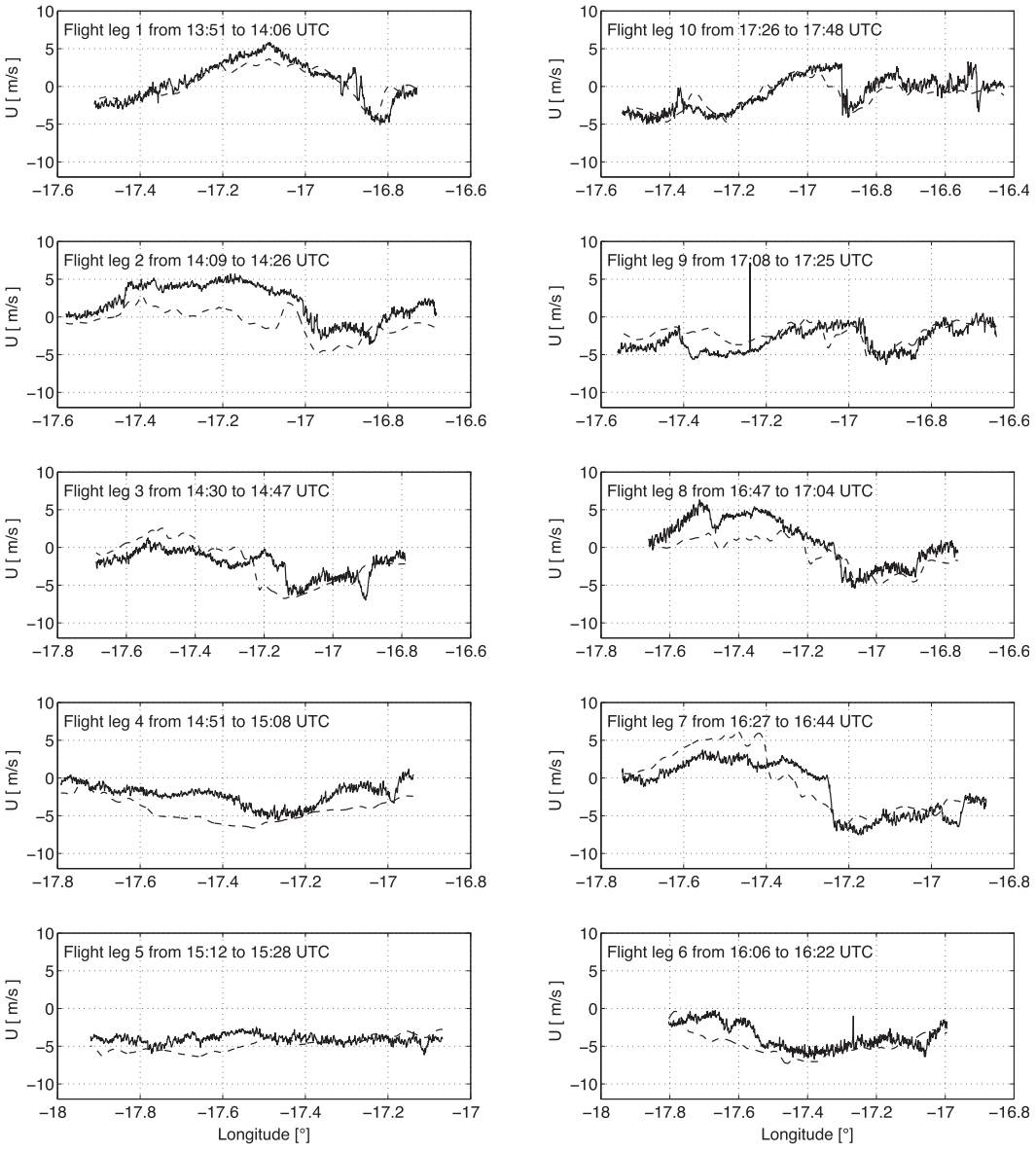

FIG. 12. As in Fig. 11, but for the cross-stream wind component.

hypothesis, a sensitivity run was performed using the free-slip boundary condition (cf. section 3b). In Fig. 16, the potential vorticity and potential temperature from this sensitivity run are shown at the same time and altitude as those from the control run. In both results, a strong unstable wake is evident and the PV magnitudes are comparable. This indicates that bottom friction is a negligible contributor to the overall vorticity and potential vorticity generation in this case. Instead, as in Grubišić et al. (1995), the bottom friction appears to have a weak dissipative effect in reducing the sharpness and magnitude of the PV anomalies farther away from the source region.

Throughout the analyzed period (1–3 September 2010), PV of variable strength is produced near the steep coasts of Madeira. Given very few clouds in our case, also the results from Minder et al. (2013) for the Caribbean island of Dominica that show the rainfall and latent heating in clouds over the island having only a secondary role in the dynamics and thermodynamics of the wake region, we eliminate the diabatic processes as a source of PV in the wake of Madeira. Since the generation of PV by surface friction in our case is rather weak, if not negligible, this leaves dissipation within local mixing zones, such as hydraulic jumps at the flank of the obstacle, as the main contributor to the leeward PV

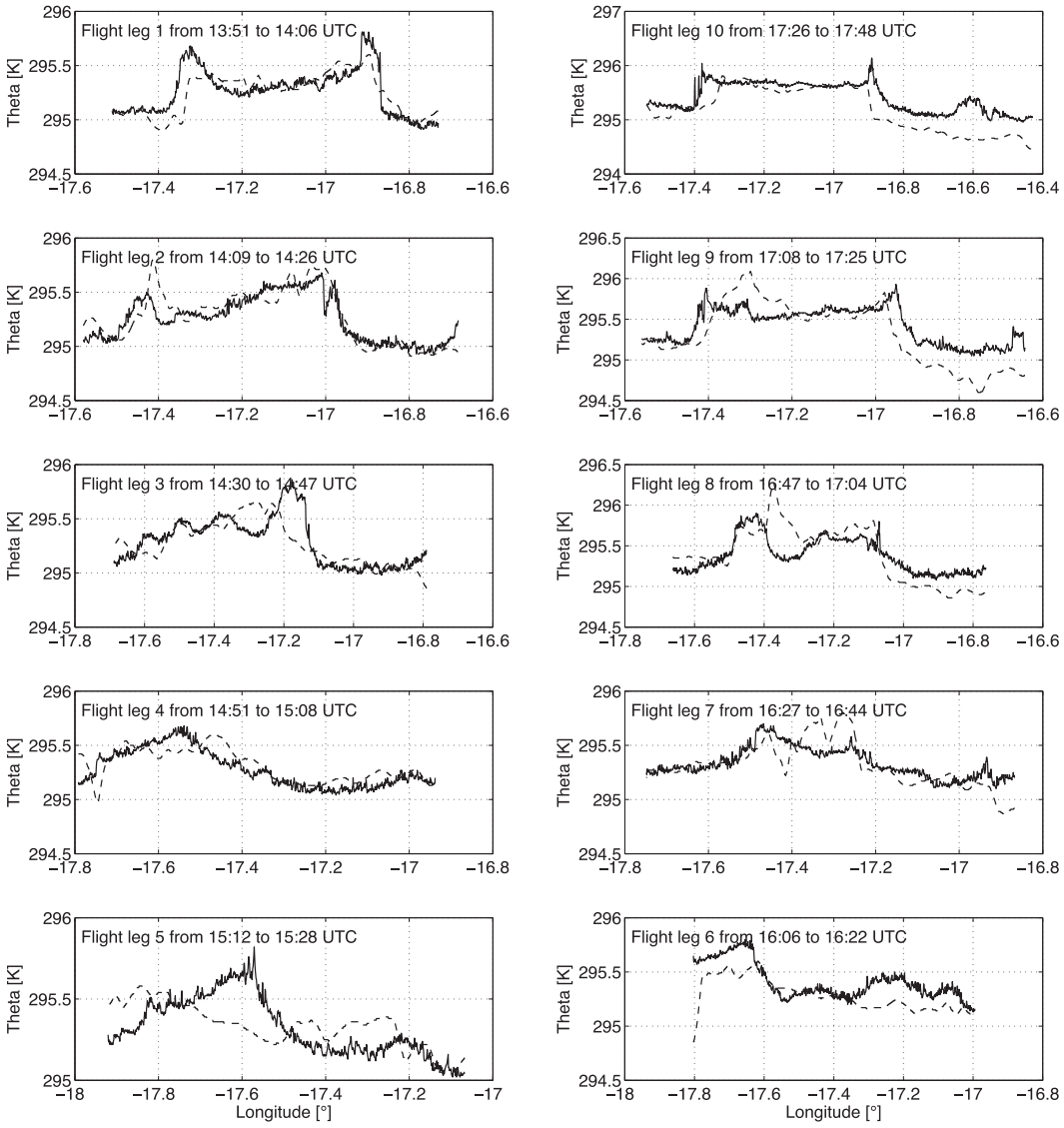

FIG. 13. As in Fig. 11, but for potential temperature.

dipole as in Schär and Smith (1993a). Indeed, formation of eddies with strong PV signatures near the flanks of Madeira occurs coincidentally with hydraulic-jump-like features and high values of turbulent kinetic energy (TKE) there.

These hydraulic-jump-like features are illustrated in Fig. 17, which shows an along-flow vertical cross section over the eastern flank of Madeira that extends along the southern shear line of the wake illustrated Fig. 15. It is evident from Fig. 17 that these jumplike features are embedded within the MBL and involve only the lowest portion of the upstream inversion. Specifically, in Fig. 17a we see the 296-K isentrope undergoing a large excursion downward over the southern flank of Madeira, followed by a sharp rebound and some residual undulations farther downwind. The model-predicted TKE in this vertical cross section reaches very high values in the zones of maximum steepness of the isentropes over the flank of Madeira and within the jump. The zone of reduced horizontal momentum (Fig. 17a) and increased TKE (Fig. 17c) extends downwind of the jump and is confined entirely below the inversion. For the process of vertical vorticity production within the hydraulic jumps, we refer the reader to Rotunno and Smolarkiewicz (1995).

c. *Eddy shedding period*

The method used in this study to determine the shedding period of Madeira's wake—the time it takes for a pair of eddies, one cyclonic and one anticyclonic, to be formed and shed from the island—is based on the

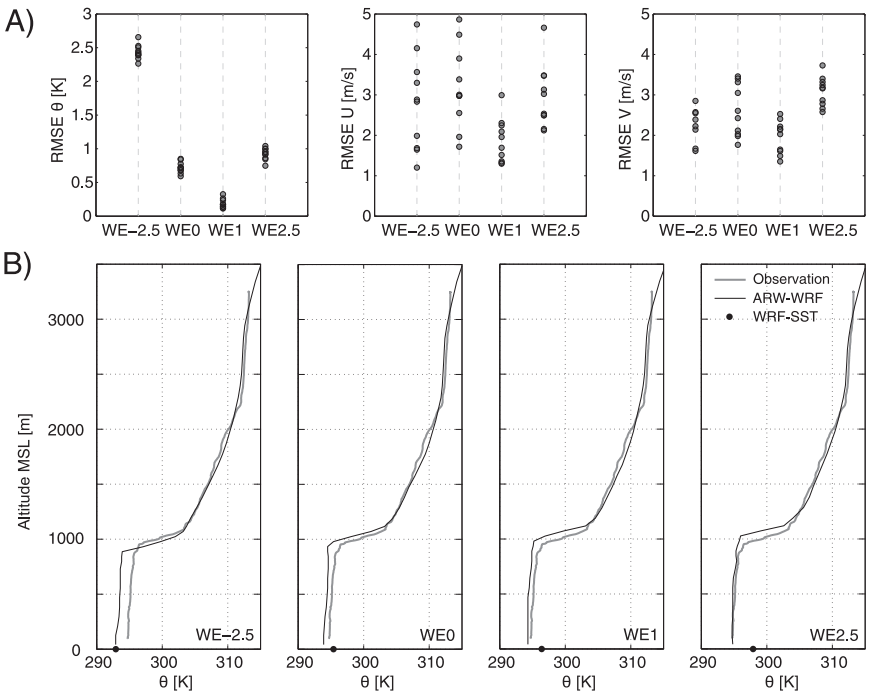

FIG. 14. Results of the SST sensitivity experiments: (a) RMSE values of (left to right) potential temperature θ and horizontal wind components u and v along the 10 wake flight legs of IWAKE45. (b) WRF-simulated (black) and observed (gray) vertical profiles of potential temperature upstream of Madeira for the four SST sensitivity experiments. Black dot indicates the SST value in each of the WRF runs.

computation of root-mean-square error [Eq. (2)] of the horizontal wind speed components and potential temperature along the 10 wake flight legs for different time lags between the observations and the model output. One expects the RMSE values to reach a minimum when the observed and the modeled vortex streets are in phase. Likewise, the RMSE maximum is expected when the observed and modeled vortex streets are out of phase by half of the shedding period. The RMSE for each wake flight leg was computed for different time lags over the interval $[-32, +6]$ h at 15-min increments. The results using the control run output are shown in Fig. 18.

As expected, the shedding frequency signal is almost absent for the along-stream velocity component and

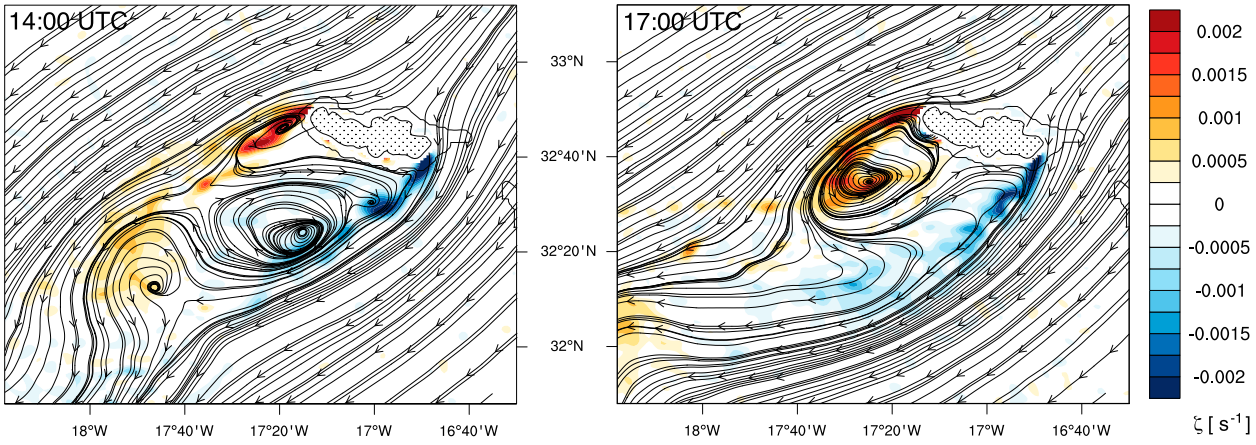

FIG. 15. Streamlines and vertical vorticity (color shading, s^{-1}) from the control run at MSL at (a) 1400 and (b) 1700 UTC 2 Sep 2010. Thick irregular lines mark the island's coastline, and enclosed dotted areas indicate terrain above 600 m.

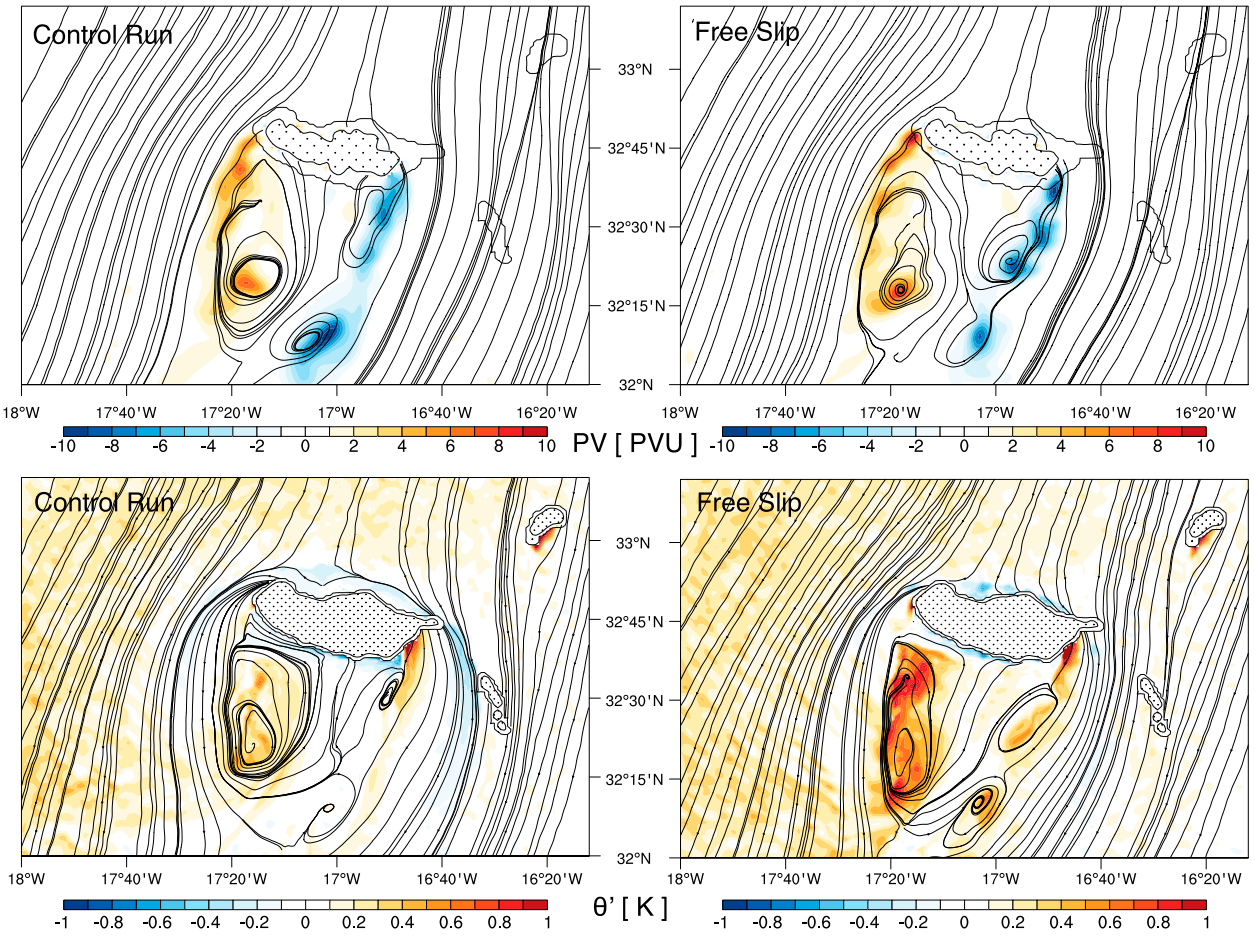

FIG. 16. (top) Potential vorticity (PVU, colored shading) at 600 m MSL and (bottom) potential temperature (K) perturbation at 50 m MSL at 1200 UTC 1 Sep 2010 from (left) the control run and (right) the free-slip sensitivity experiment. The perturbation is with respect to the domain-average potential temperature at this level.

strong in the cross-stream velocity component—the velocity component that carries the information about the phase of shedding. The RMSE for the cross-stream wind component gives a shedding period of 7–8 h. This result agrees to what one gets from the spectral analysis of the time series for the cross-stream velocity component and is corroborated by the visual inspection of the model simulations. On the other hand, the shedding period based on the RMSE for potential temperature is closer to 12 h. It appears that the potential temperature signal of wake eddies at the altitude of the wake flight legs is masked by a much stronger signal of the diurnal temperature variation within the boundary layer.

6. Summary and conclusions

The first aerial observations of the atmospheric wake of Madeira, presented in this study, reveal a strong and unsteady wake leeward of this large subtropical island. The in situ and remotely sensed observations presented here were obtained by the SAFIRE ATR-42 research aircraft during the I-WAKE campaign, which was conducted in Madeira in August–September 2010. The attendant numerical simulations were carried out with the ARW model.

The detailed observations of the 2 September 2010 Madeira wake event from the IWAKE44 and IWAKE45 research flights presented in this study provide the extensive coverage of the atmospheric wake of Madeira, extending the analysis some 50 km upwind and 120 km downstream of the island.

The sounding obtained upstream of the island during the IWAKE44 shows a two-layer atmospheric structure, with a sharp trade wind inversion below the mountain top, at approximately 1 km MSL, separating a well-mixed MBL from a stably stratified layer aloft. While our climatological analysis of the MBL inversion heights shows some variation of the inversion height during

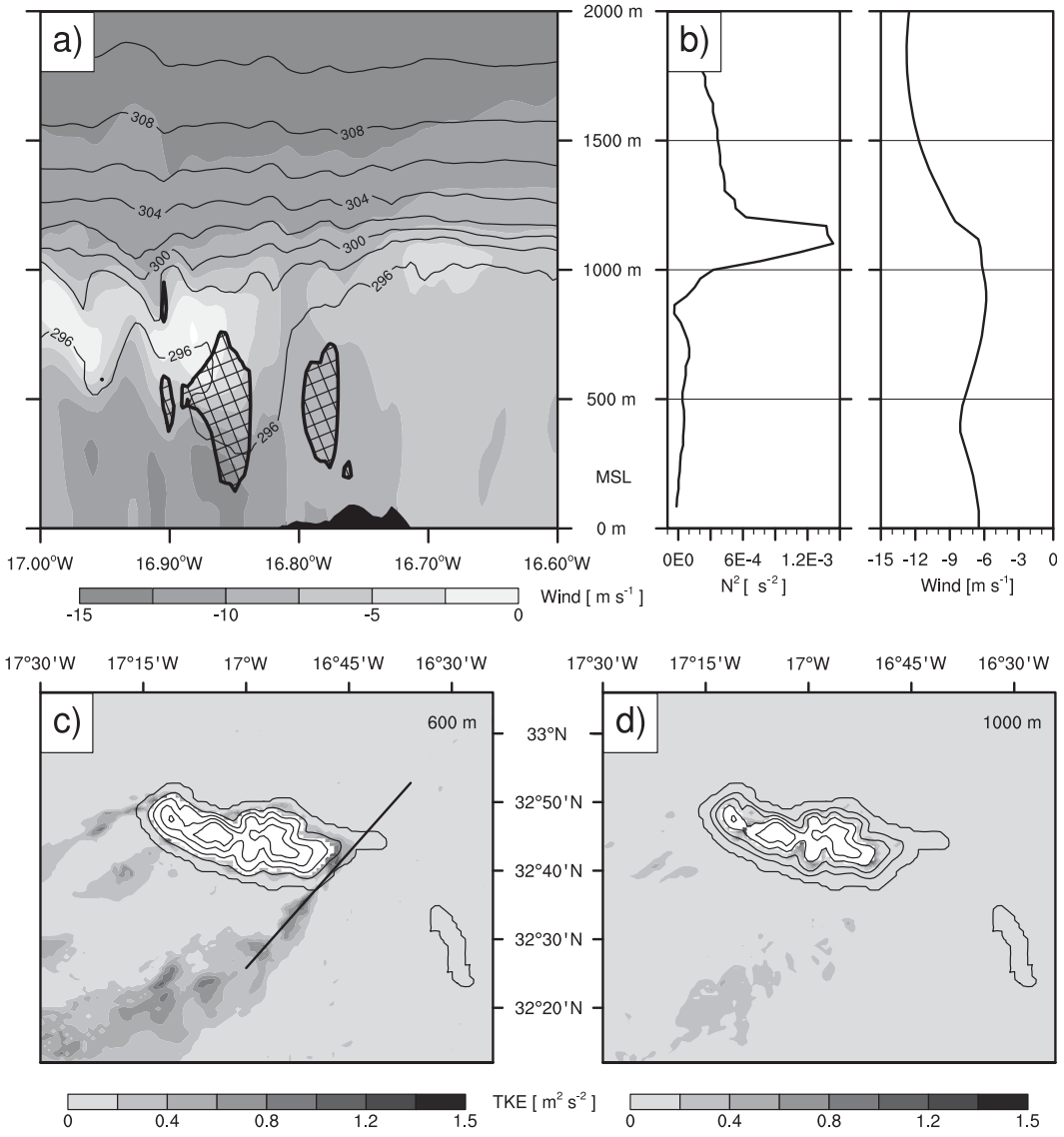

FIG. 17. Hydraulic-jump-like features in the flow past Madeira at 1700 UTC 2 Sep 2010: (a) isentropes (solid lines), section-parallel wind speed (grayscale), and subgrid-scale TKE $> 0.75\,\mathrm{m^2\,s^{-1}}$ (hatching), in a vertical cross section over the eastern flank of Madeira. (b) Vertical profiles of the (left) Brunt–Väisälä frequency (N^2) and (right) horizontal wind speed at the upstream end of (a). The model-predicted TKE in horizontal planes at (c) 600 and (d) 1000 m MSL. The base of the vertical cross section in (a) is shown in (c). The terrain contour interval in (c) and (d) is 300 m.

summer months, 1000 m MSL is a rather typical height at which one finds the MBL inversion in the June–September period, leading us to conclude that the conditions on 2 September 2010 are representative for most of the days during summer.

The observations collected downwind of Madeira during the IWAKE45 flight reveal distinctive atmospheric wake signatures, including strong lateral wind shear zones and warm and dry leeside eddies. Within the wake region, a strong momentum deficit was observed yet no indication of steadiness of the wake circulations was found. Furthermore, a strong anticorrelation of the wind speed and the sea surface temperature (SST) was detected within the wake, with positive SST wake anomalies of greater than 2 K closest to the island. The likely origin of these SST anomalies is the reduced vertical mixing of the ocean surface layer, resulting from a reduced surface wind stress there. The strongest observed anticorrelation between the SST and the wind in the immediate lee of the island is likely the reflection of the thermal inertia of the ocean, allowing it to retain the ''memory'' of the prevailing cloud-free conditions

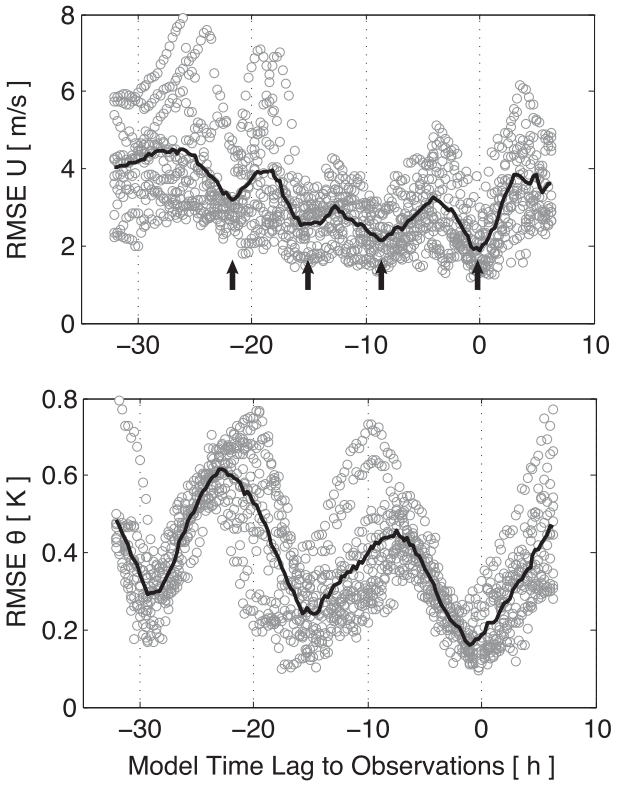

FIG. 18. RMSE for the cross-stream (top) horizontal wind component and (bottom) potential temperature for the 10 wake flight legs computed for different time shifts $\Delta t = t_{sim} - t_{obs}$ between the observations and the model output. Negative time shifts indicate the observations lagging behind the model output and vice versa. The solid line shows the ensemble mean.

there due to the downwelling of air in the steady near wake (cf. Fig. 1). The observed anticorrelation between the SST and wind speed is in agreement with previous studies that show distinct diurnal SST anomalies in calm regions disappearing with the onset of wind stress on the ocean surface due to enhanced vertical mixing (Kawai and Wada 2007).

The high-resolution numerical simulations with the WRF Model of the flow past Madeira during the period of 1–3 September 2010 were used to study the dynamics of wake generation and its temporal evolution. The analysis of the atmospheric structure upwind of the island shows an evolution from a deep uniformly stratified atmosphere at the beginning of this period toward the described two-layer structure during the time of the observations. The numerical simulations reveal a strong and unstable atmospheric wake in the lee of Madeira at the time of observations on 2 September. The comparison of the model predictions and the observations shows a remarkable fidelity of the wake features simulated by WRF. Surprisingly, the model does not only capture the oscillation frequency of the unstable wake correctly but also the phase of the oscillation. Within the simulated wake, strong vertical vorticity and potential vorticity (PV) anomalies are found within the marine boundary layer (MBL), emanating from the flanks of the island. The PV production there appears to be associated with the dissipation in the highly turbulent hydraulic-jump-like flow features within the MBL. The shedding period of the simulated wake of Madeira was found to be close to 7–8 h. This eddy shedding period agrees with an early estimate by Chopra and Hubert (1965), who obtained approximately 7 h by applying a kinematic method to the analysis of satellite images. On the other hand, a recent numerical study by Nunalee and Basu (2014) of another Madeira wake case estimates the shedding period to be approximately 5 h.

The performed sensitivity experiments reveal a strong impact of SST on the atmospheric stratification, with higher SSTs leading to a deeper and slightly warmer MBL with a sharper inversion at its top. These relatively modest changes to the upstream stratification over the examined range of SSTs nevertheless have a measurable impact on the fidelity of the wake simulations, in particular on the cross-stream velocity component that carries most of the information on details of the wake circulation, including the position of the wake eddies and the phase of the eddy shedding. The sensitivity experiments with surface friction show bottom friction to be a negligible source of vertical vorticity within the wake yet to have a dissipative effect on the wake flow as in the shallow-water simulations of Grubišić et al. (1995).

Acknowledgments. The I-WAKE project was funded by the European Facility for Airborne Research (EUFAR), an ''Integrating Activity'' funded by the European Commission under FP5/FP6/FP7. We are grateful for the professionalism and commitment of the SAFIRE (''Service des Avions Français Instruments pour la Recherche en Environnement'') operational team during the preparation and execution of the I-WAKE field campaign. CIIMAR's financial office provided valuable support for the field campaign. We thank the Madeira Airport NAV team for providing flexible and efficient air traffic support and flight information during the I-WAKE campaign. The Porto Santo Airport administration office was also very helpful with the local logistics. Ricardo Tomé participated in the construction of the CIIMAR's MM5 forecasting system that was used in flight planning (http://wakes.uma.pt). Forecasts were produced at CIIMAR's HPC unit that was acquired using FCT pluriannual funds (PesT-C/MAR/LA0015/2011). The satellite climatology of Madeira's wake was created by Brigitta Goger as part of her Bachelor thesis

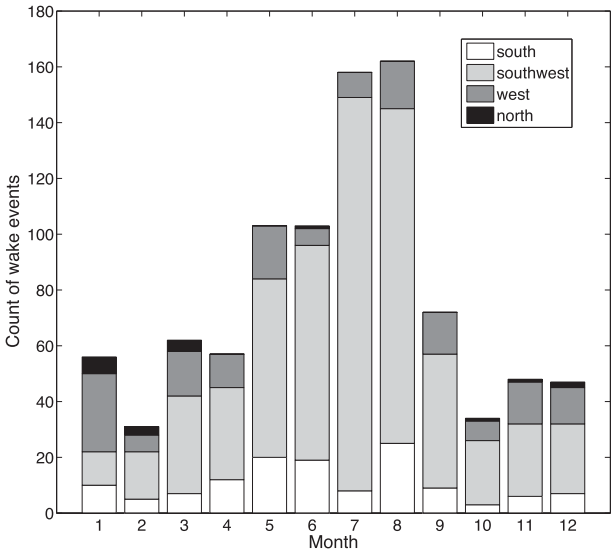

FIG. A1. Total number of days with a wake leeward of Madeira based on the visible satellite imagery from 2003 to 2010. The number of wake days is shown as a function of month and the orientation of the wake axis. There are 115 days yr^{-1} on average with a wake visible downwind of Madeira.

at the University of Vienna. We thank Richard Rotunno for many stimulating discussions on the vorticity generation and two anonymous reviewers for their comments that have helped us improve the presentation. This research has been supported in part by the EU FP7-PEOPLE-2009-RG 256511 Grant to the University of Vienna.

APPENDIX

Satellite Climatology of Madeira's Wakes

Our climatological analysis of wakes in the lee of Madeira is based on the visible and infrared imagery from NOAA's polar-orbiting satellites obtained from the SATMOS Archive Center (MeteoFrance). The primary dataset used in this analysis is the visible imagery from the time period 2003–10. Days with a wake event visible in the stratocumulus cloud deck leeward of Madeira were identified and categorized according to the wake type and the orientation of the wake axis (south, southwest, west, north). Three wake types were identified: (i) a strong unstable, indicated by the presence of a vortex street; (ii) a strong stable, indicated by the presence of a bow cloud and a symmetric recirculation zone in the lee; and (iii) a weak wake, indicated by a long reduced momentum zone in the lee with no obvious signs of instability. The two wake descriptors, the orientation and the type, are interpreted as indicative, respectively, of the wind direction and the combined effect of the upstream wind speed and the inversion height. Clearly, wakes under cloud-free conditions are not included in the total count. Consequently, our numbers represent an underestimate of the total number of days with wakes in the lee of Madeira. However, under an assumption that the cloud-free days are distributed approximately uniformly throughout the year, this underestimate should not affect the annual distribution.

Figure A1 shows the annual distribution of the total number of days with a wake event over the analyzed 8-yr period for different wake orientations. The results show a larger number of wake events from May to September with a late summer maximum in August. The asymmetry in the annual distribution of wake events is consistent with the asymmetry of the annual variation of the MBL inversion height (cf. Fig. 3) discussed in section 2b. As expected, the dominant direction of the wake is to the southwest, corresponding to the dominant northeast direction of the trade winds, caused by the eastern branch of the Azores high. From October through April, synoptic conditions show more variability, as reflected in the large number of wakes oriented in different directions, and conditions that are overall less conductive to wake generation.

REFERENCES

Caldeira, R. M. A., and R. Tomé, 2013: Wake response to an ocean-feedback mechanism: Madeira island case study. *Bound.-Layer Meteor.*, **148**, 419–436, doi:10.1007/s10546-013-9817-y.

Chopra, K. P., and L. F. Hubert, 1965: Mesoscale eddies in wake of islands. *J. Atmos. Sci.*, **22**, 652–657, doi:10.1175/1520-0469(1965)022<0652:MEIWOI>2.0.CO;2.

Davis, R., B. Hayden, D. Gay, W. L. Phillips, and G. Jones, 1997: The North Atlantic subtropical anticyclone. *J. Climate*, **10**, 728–744, doi:10.1175/1520-0442(1997)010<0728:TNASA>2.0.CO;2.

Epifanio, C. C., and D. Durran, 2002a: Lee-vortex formation in free-slip stratified flow over ridges. Part I: Comparison of weakly nonlinear inviscid theory and fully nonlinear viscous simulations. *J. Atmos. Sci.*, **59**, 1153–1165, doi:10.1175/1520-0469(2002)059<1153:LVFIFS>2.0.CO;2.

——, and ——, 2002b: Lee-vortex formation in free-slip stratified flow over ridges. Part II: Mechanisms of vorticity and PV production in nonlinear viscous wakes. *J. Atmos. Sci.*, **59**, 1166–1181, doi:10.1175/1520-0469(2002)059<1166:LVFIFS>2.0.CO;2.

Etling, D., 1989: On atmospheric vortex streets in the wake of large islands. *Meteor. Atmos. Phys.*, **41**, 157–164, doi:10.1007/BF01043134.

Gill, A. E., 1982: *Atmosphere–Ocean Dynamics.* Academic Press, 662 pp.

Grubišić, V., R. B. Smith, and C. Schär, 1995: The effect of bottom friction on shallow-water flow past an isolated obstacle. *J. Atmos. Sci.*, **52**, 1985–2005, doi:10.1175/1520-0469(1995)052<1985:TEOBFO>2.0.CO;2.

Hong, S.-Y., and J.-O. J. Lim, 2006: The WRF single-moment 6-class microphysics scheme (WSM6). *J. Korean Meteor. Soc.*, **42**, 129–151.

Hubert, L. F., and A. F. Krueger, 1962: Satellite pictures of mesoscale eddies. *Mon. Wea. Rev.*, **90**, 457–463, doi:10.1175/1520-0493(1962)090<0457:SPOME>2.0.CO;2.

Iacono, M. J., J. S. Delamere, E. J. Mlawer, M. W. Shephard, S. A. Clough, and W. D. Collins, 2008: Radiative forcing by long-lived greenhouse gases: Calculations with the AER radiative transfer models. *J. Geophys. Res.*, **113**, D13103, doi:10.1029/2008JD009944.

Janjić, Z. I., 1994: The step-mountain eta coordinate model: Further developments of the convection, viscous sublayer, and turbulence closure schemes. *Mon. Wea. Rev.*, **122**, 927–945, doi:10.1175/1520-0493(1994)122<0927:TSMECM>2.0.CO;2.

Jiang, Q., 2014: Application of reduced-gravity shallow-water theory to atmospheric flow over topography. *J. Atmos. Sci.*, **71**, 1460–1479, doi:10.1175/JAS-D-13-0101.1.

Kawai, Y., and A. Wada, 2007: Diurnal sea surface temperature variation and its impact on the atmosphere and ocean: A review. *J. Oceanogr.*, **63**, 721–744, doi:10.1007/s10872-007-0063-0.

Minder, J. R., R. B. Smith, and A. Nugent, 2013: The dynamics of ascent-forced orographic convection in the tropics: Results from Dominica. *J. Atmos. Sci.*, **70**, 4067–4088, doi:10.1175/JAS-D-13-016.1.

Mlawer, E., J. Steven, J. Taubman, P. D. Brown, M. J. Iacono, and S. A. Clough, 1997: Radiative transfer for inhomogeneous atmospheres: RRTM, a validated correlated-k model for the longwave. *J. Geophys. Res.*, **102**, 16 663–16 682, doi:10.1029/97JD00237.

Nickerson, E. C., and M. A. Dias, 1981: On the existence of atmospheric vortices downwind of Hawaii during the HAMEC project. *J. Appl. Meteor.*, **20**, 868–873, doi:10.1175/1520-0450(1981)020<0868:OTEOAV>2.0.CO;2.

Niu, G.-Y., and Coauthors, 2011: The community Noah land surface model with multiparameterization options (Noah-MP): 1. Model description and evaluation with local-scale measurements. *J. Geophys. Res.*, **116**, D12109, doi:10.1029/2010JD015139.

Nunalee, C. G., and S. Basu, 2014: On the periodicity of atmospheric von Kármán vortex streets. *Environ. Fluid Mech.*, **14**, 1335–1355, doi:10.1007/s10652-014-9340-9.

Rotunno, R., and P. K. Smolarkiewicz, 1995: Vorticity generation in the shallow-water equations as applied to hydraulic jumps. *J. Atmos. Sci.*, **52**, 320–330, doi:10.1175/1520-0469(1995)052<0320:VGITSW>2.0.CO;2.

——, V. Grubišić, and P. K. Smolarkiewicz, 1999: Vorticity and potential vorticity in mountain wakes. *J. Atmos. Sci.*, **56**, 2796–2810, doi:10.1175/1520-0469(1999)056<2796:VAPVIM>2.0.CO;2.

Schär, C., 1993: A generalization of Bernoulli's theorem. *J. Atmos. Sci.*, **50**, 1437–1443, doi:10.1175/1520-0469(1993)050<1437:AGOBT>2.0.CO;2.

——, and R. B. Smith, 1993a: Shallow-water flow past isolated topography. Part I: Vorticity production and wake formation. *J. Atmos. Sci.*, **50**, 1373–1400, doi:10.1175/1520-0469(1993)050<1373:SWFPIT>2.0.CO;2.

——, and ——, 1993b: Shallow-water flow past isolated topography. Part II: Transition to vortex shedding. *J. Atmos. Sci.*, **50**, 1401–1412, doi:10.1175/1520-0469(1993)050<1401:SWFPIT>2.0.CO;2.

——, and D. Durran, 1997: Vortex formation and vortex shedding in continuously stratified flows past isolated topography. *J. Atmos. Sci.*, **54**, 534–554, doi:10.1175/1520-0469(1997)054<0534:VFAVSI>2.0.CO;2.

Scorer, R. S., 1986: *Cloud Investigation by Satellite.* Wiley, 300 pp.

Skamarock, W., and J. Klemp, 2008: A time-split nonhydrostatic atmospheric model for weather research and forecasting applications. *J. Comput. Phys.*, **227**, 3465–3485, doi:10.1016/j.jcp.2007.01.037.

Smith, R. B., and V. Grubišić, 1993: Aerial observations of Hawaii's wake. *J. Atmos. Sci.*, **50**, 3728–3750, doi:10.1175/1520-0469(1993)050<3728:AOOHW>2.0.CO;2.

——, A. C. Gleason, P. A. Gluhosky, and V. Grubišić, 1997: The wake of St. Vincent. *J. Atmos. Sci.*, **54**, 606–623, doi:10.1175/1520-0469(1997)054<0606:TWOSV>2.0.CO;2.

Smolarkiewicz, P. K., and R. Rotunno, 1989: Low Froude number flow past three-dimensional obstacles. Part I: Baroclinically generated lee vortices. *J. Atmos. Sci.*, **46**, 1154–1164, doi:10.1175/1520-0469(1989)046<1154:LFNFPT>2.0.CO;2.

Young, G. S., and J. Zawislak, 2006: An observational study of vortex spacing in island wake vortex streets. *Mon. Wea. Rev.*, **134**, 2285–2294, doi:10.1175/MWR3186.1.

Zimmermann, L. I., 1969: Atmospheric wake phenomena near the Canary Islands. *J. Atmos. Sci.*, **8**, 896–907, doi:10.1175/1520-0450(1969)008<0896:AWPNTC>2.0.CO;2.